# Supplementary Information of CP-ART-03-2019-001482.R2.

# The solid phase thermal decomposition and nano-crystal effect of hexahydro-1,3,5-trinitro-1,3,5-triazine (RDX) from ReaxFF large scale molecular dynamics simulation

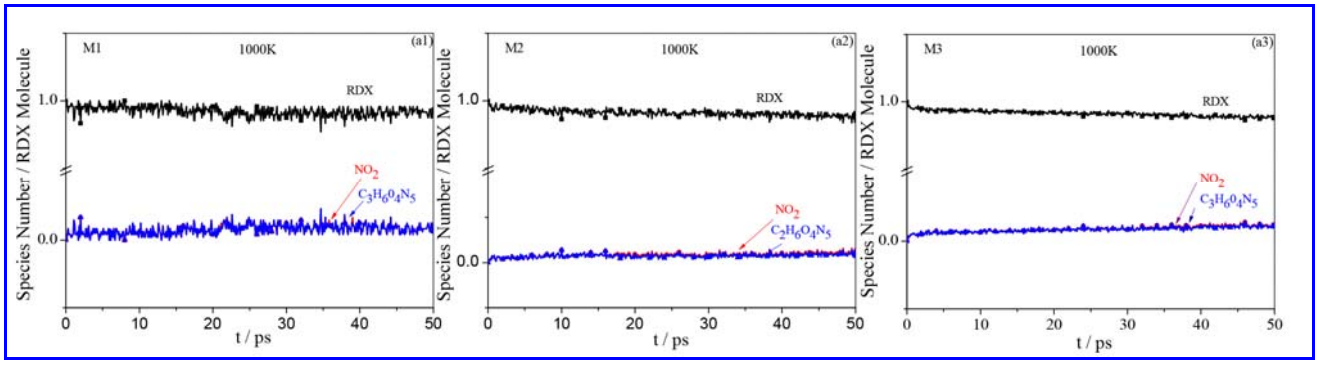


Fig. S1 Evolution of intermediate and secondary products of RDX decomposition for three models at 1000K.

video 1.gif

Video 1, Diffusing of $NO_2$ in M1 in solid phase decay stage at 3000K

video 2.gif

Video 2, Diffusing of $NO_2$ in M2 in solid phase decay stage at 3000K

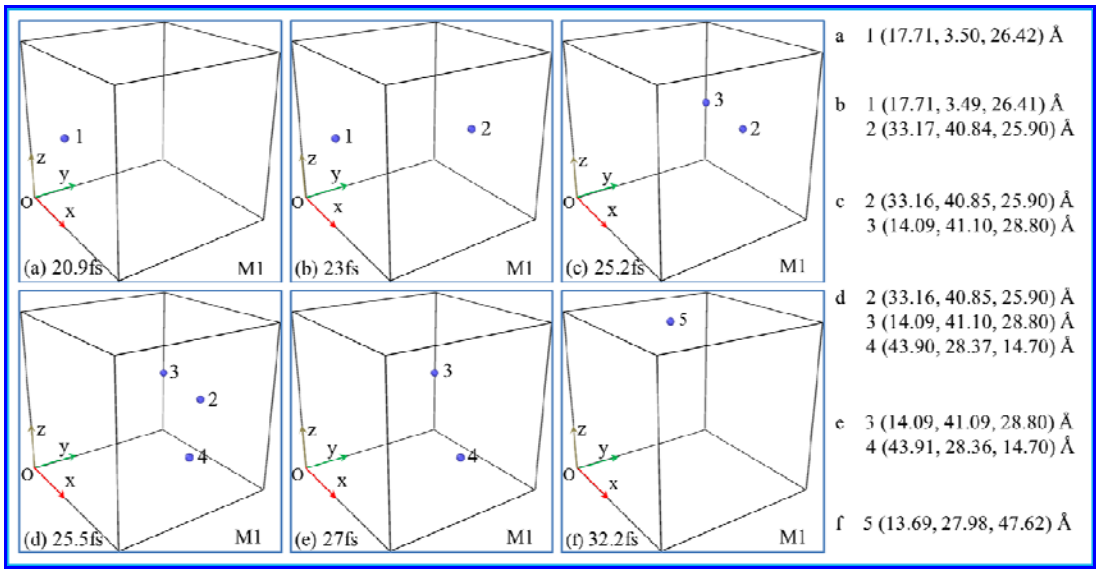


Figure S2 Spatial distribution and 3D space coordinates of $NO_2$ in M1 at 2000K at the initial time with step-time of 0.1fs

(a, b, c, d, e, f is at the time of 20.9fs, 23.0fs, 25.2fs, 25.5fs, 27fs, 32.2fs, respectively).

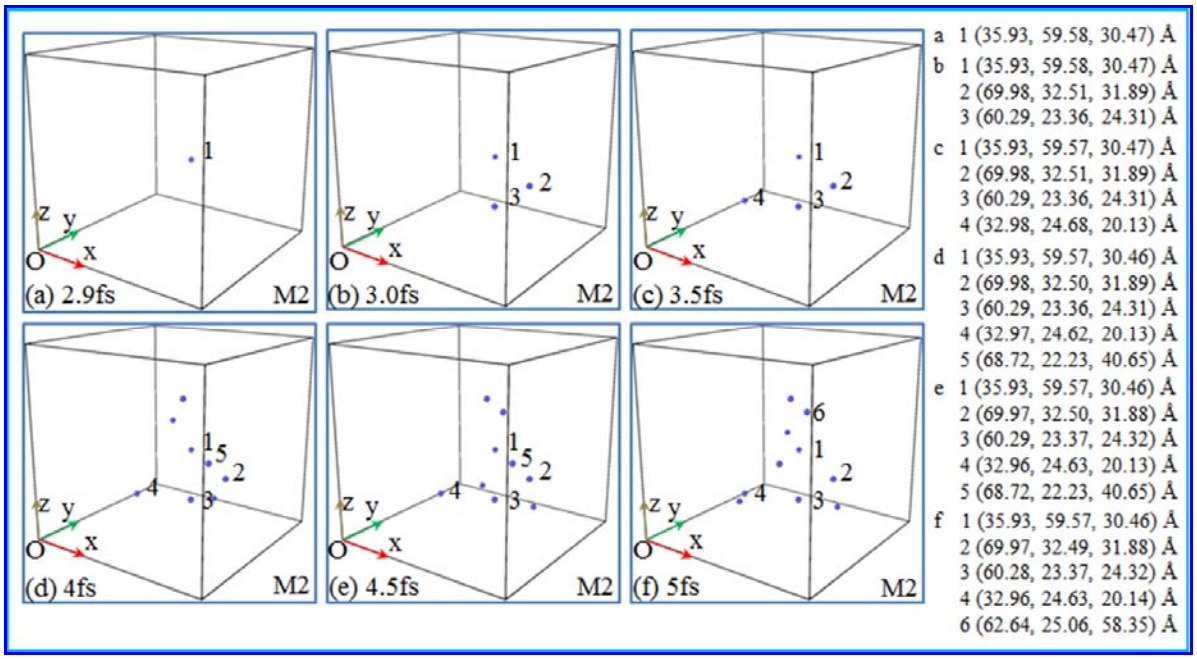


Figure S3 Spatial distribution and 3D space coordinates of $NO_2$ in M2 at 3000K at the initial time with step-time of 0.1fs (a, b, c, d, e, f is at the time of 2.9fs, 3.0fs, 3.5fs, 4.0fs, 4.5fs, 5.0fs, respectively).

Table S1, Reactions with the Highest Frequencies of M1, M2 under 2000K during 0-15ps with an account step-time of 10fs.

| M1 | | | M2 | | |
|---|---|---|---|---|---|
| Occupies | times | Reaction | Occupies | times | Reaction |
| 24.70% | 205 | $C_3H_6O_6N_6 \rightarrow C_3H_6O_4N_5 + NO_2$ | 24.99% | 807 | $C_3H_6O_6N_6 \rightarrow C_3H_6O_4N_5 + NO_2$ |
| 18.19% | 151 | $CH_2O_2N_2 \rightarrow CH_2N + NO_2$ | 16.01% | 517 | $CH_2O_2N_2 \rightarrow CH_2N + NO_2$ |
| 10.72% | 89 | $C_3H_6O_4N_5 \rightarrow C_3H_6O_2N_4 + NO_2$ | 11.12% | 359 | $C_3H_6O_4N_5 \rightarrow C_3H_6O_2N_4 + NO_2$ |
| 9.88% | 82 | $C_2H_4O_2N_3 \rightarrow CH_2N + CH_2O_2N_2$ | 9.01% | 291 | $C_2H_4O_2N_3 \rightarrow CH_2N + CH_2O_2N_2$ |
| 8.67% | 72 | $C_3H_6O_4N_5 \rightarrow C_2H_4O_2N_3 + CH_2O_2N_2$ | 8.95% | 289 | $C_3H_6O_4N_5 \rightarrow C_2H_4O_2N_3 + CH_2O_2N_2$ |
| 6.27% | 52 | $C_3H_6O_2N_4 \rightarrow C_3H_6N_3 + NO_2$ | 7.71% | 249 | $C_3H_6O_2N_4 \rightarrow C_3H_6N_3 + NO_2$ |
| 3.73% | 31 | $CH_2N + NO_2 \rightarrow CHN + HONO$ | 3.93% | 127 | $CH_2N + NO_2 \rightarrow CHN + HONO$ |
| 2.29% | 19 | $NO_2 + NO_2 \rightarrow N_2O_4$ | 2.42% | 78 | $C_3H_6N_3 \rightarrow C_2H_4N_2 + CH_2N$ |
| 2.29% | 19 | $C_3H_6N_3 \rightarrow C_2H_4N + CH_2N_2$ | 1.80% | 58 | $NO_2 + NO_2 \rightarrow N_2O_4$ |
| 1.93% | 16 | $N_2O_4 \rightarrow NO_3 + NO$ | 1.80% | 58 | $C_3H_6O_2N_4 \rightarrow C_3H_6N_3 + NO_2$ |
| 1.69% | 14 | $C_3H_6N_3 \rightarrow C_2H_4N_2 + CH_2N$ | 1.61% | 52 | $NO_2 + NO_2 \rightarrow NO_3 + NO$ |
| 1.33% | 11 | $C_3H_6O_2N_4 \rightarrow C_3H_6N_3 + NO_2$ | 1.58% | 51 | $N_2O_4 \rightarrow NO_3 + NO$ |
| 1.20% | 10 | $C_3H_6O_4N_5 \rightarrow CH_2N + 2CH_2O_2N_2$ | 1.49% | 48 | $C_2H_4O_2N_3 \rightarrow C_2H_4N_2 + NO_2$ |
| 1.20% | 10 | $C_3H_6O_2N_4 \rightarrow C_2H_4N_2 + CH_2O_2N_2$ | 1.49% | 48 | $C_3H_6N_3 \rightarrow C_2H_4N + CH_2N_2$ |
| 1.08% | 9 | $C_3H_6O_4N_5 \rightarrow C_3H_6N_3 + 2NO_2$ | 1.33% | 43 | $C_3H_6N_3 + NO_2 \rightarrow C_3H_5N_3 + HONO$ |
| 1.08% | 9 | $CH_2N_2 + NO_2 \rightarrow CHN_2 + HONO$ | 1.05% | 34 | $C_3H_6O_4N_5 \rightarrow C_3H_6N_3 + 2NO_2$ |

| | | | | | |
|---|---|---|---|---|---|
| 0.96% | 8 | $C_3H_6O_6N_6 \rightarrow C_3H_6O_2N_4 + 2NO_2$ | 1.02% | 33 | $C_3H_6O_2N_4 + NO_2 \rightarrow C_3H_5O_2N_4 +$ HONO |
| 0.96% | 8 | $C_3H_6N_3 + NO_2 \rightarrow C_3H_5N_3 + HONO$ | 0.96% | 31 | $C_3H_5O_4N_5 \rightarrow C_3H_5O_2N_4 + NO_2$ |
| 0.96% | 8 | $C_3H_5N_3 + NO_2 \rightarrow C_3H_4N_3 + HONO$ | 0.93% | 30 | $C_3H_6O_4N_5 \rightarrow CH_2N + 2CH_2O_2N_2$ |
| 0.84% | 7 | $NO_2 + NO_2 \rightarrow NO_3 + NO$ | 0.81% | 26 | $C_2H_3N_2 \rightarrow CH_2N +$ CHN |

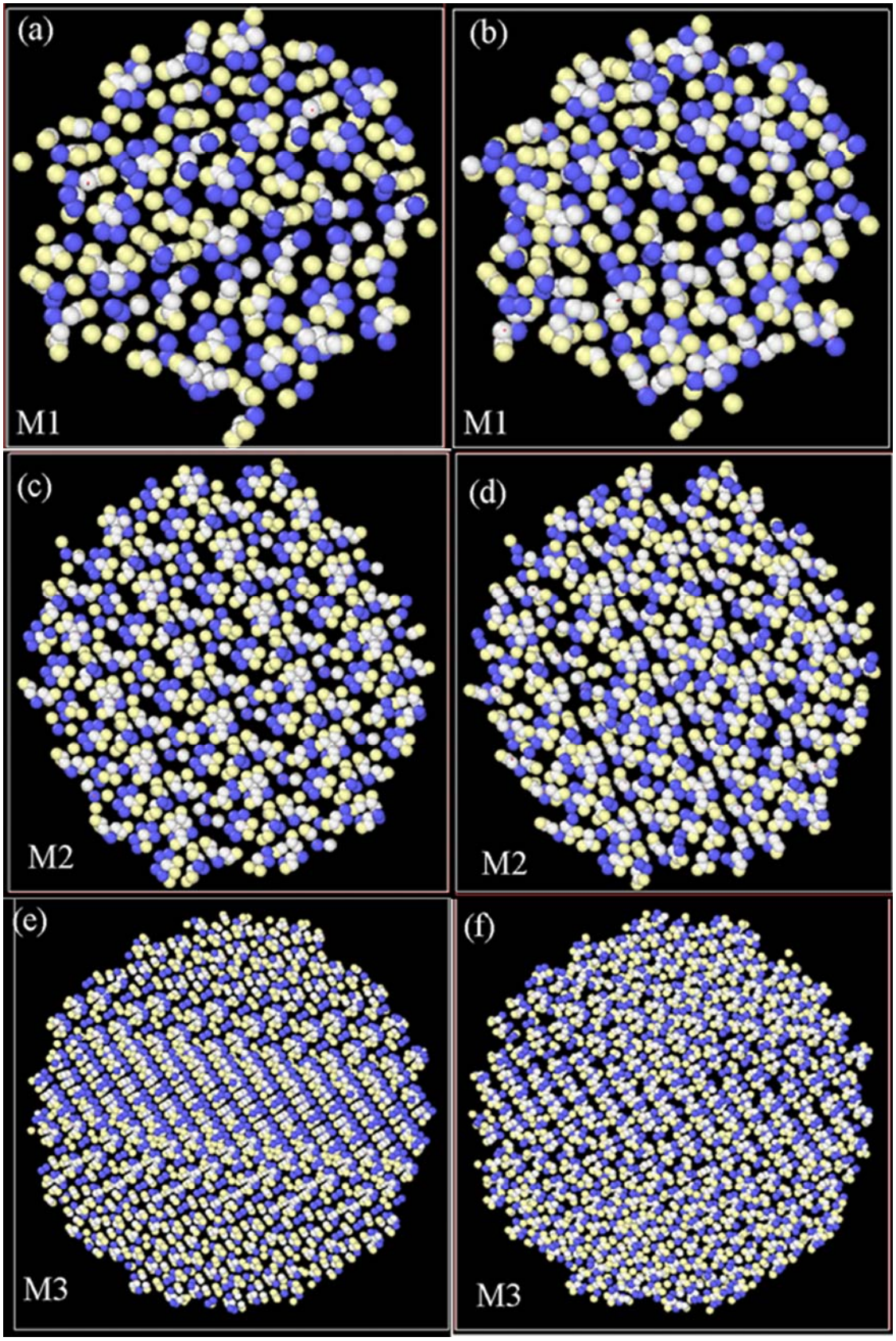


Figure. S4, Detailed structure (without circles marks) of a slice of 3 Å thickness cut from nano RDX particle models before relaxing and that of the same position after relaxing at 300K and 1.0 atmosphere pressure (a: M1 before relaxed, b: M1 after relaxed, c: M2 before relaxed, d: M2 after relaxed, e: M3 before relaxed, f: M3 after relaxed).

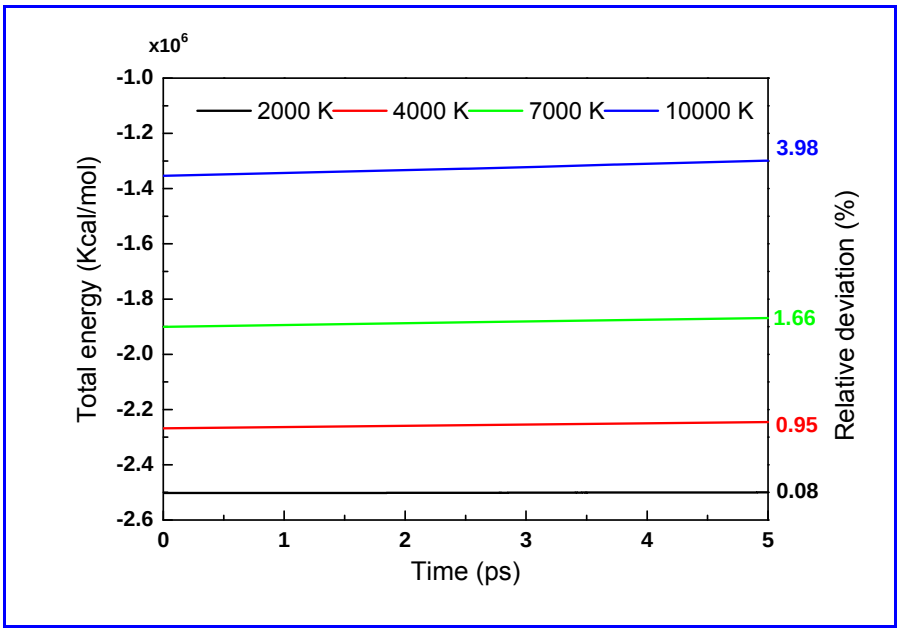


Fig. S5. Total energy evolution and relative deviation of systems with different temperatures.

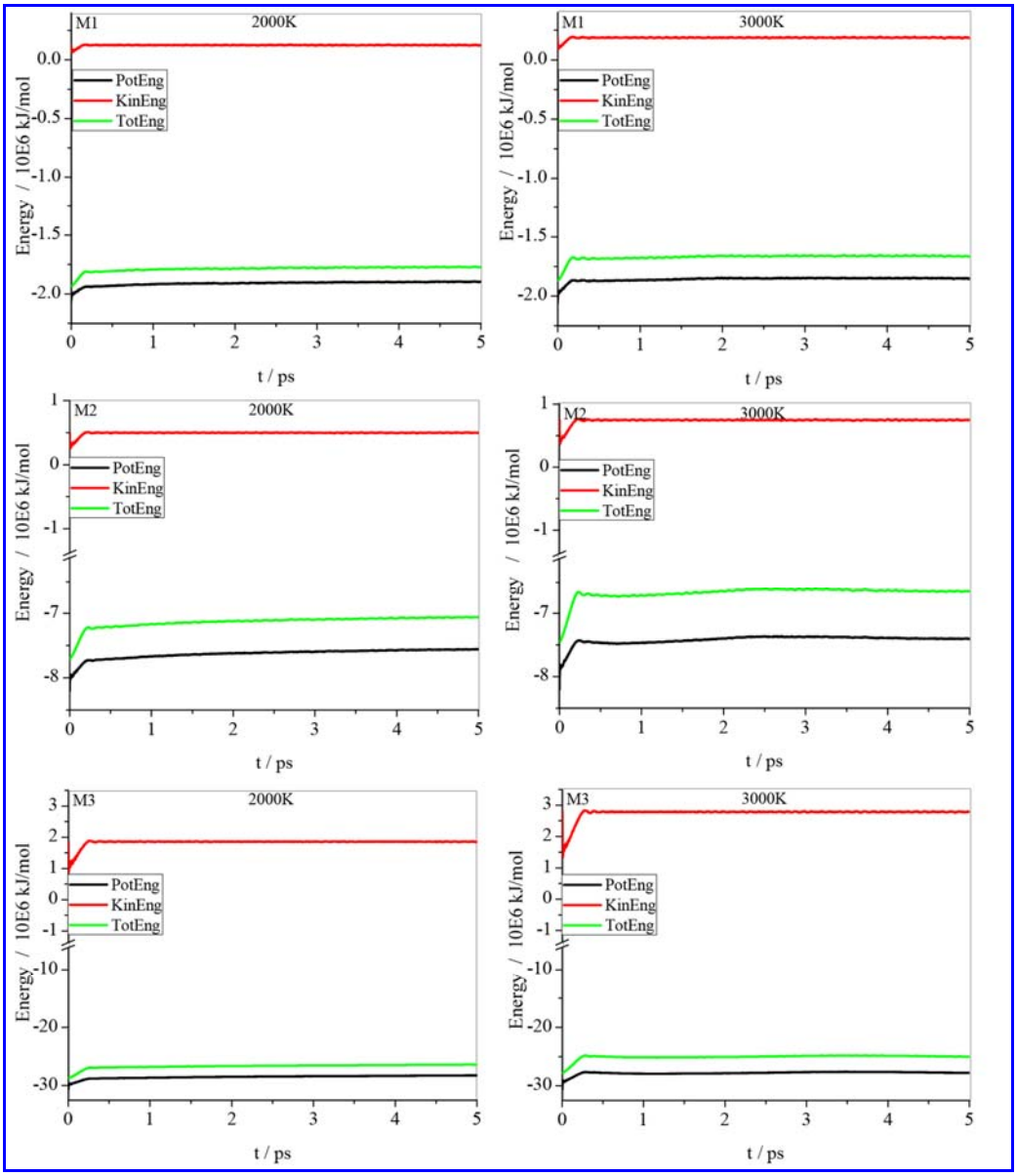


Fig. S6. Energy evolutions of M1,M2,M3 systems with different temperatures during the first 5 ps NVT simulations.

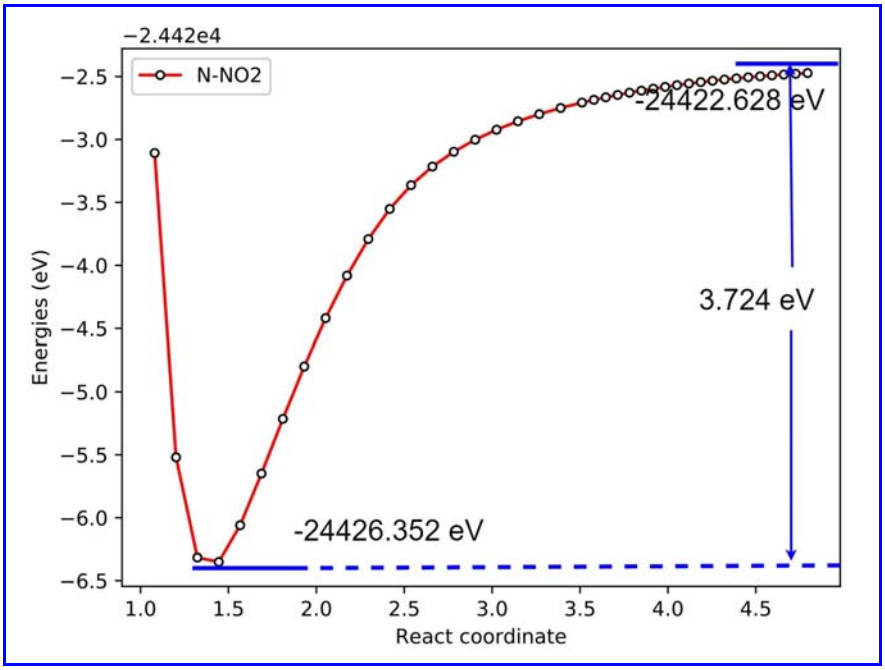


Fig. S7. N−$NO_2$ fission dynamics of RDX on the surface of the particle at a sampling temperature of 1750 K.

## Discussion about how the mechanism would change if the shape of particles changes

*As well known, the ratio of surface to volume in sphere is minimum compare with other shapes, such as cubic, needle, prism or gem shape. So if the molecular number of a single RDX crystal keeps same and the crystal shape changes to any other shape, the molecular number on the crystal surface will increase obviously. Thus base on the quantum-chemical studies by Liu, Zhu and Xiao (J. Phys. Chem. C 2016, 120, 27182−27191), the excess energy in the whole particle will increasing. We believe that the more the excess energy will be transfer into the whole crystal under the energy distribution mechanism driven by phonon vibrations founded in this manuscript, and cause a series of effect on decomposition reactions. So there will be bigger probability in higher energy barrier reactions, faster crystal decay, faster $NO_2$ diffusing, and bigger kinetic rate.*

*Furthermore, the change of crystal shape also could cause big effect on stacking density or filling of the reaction volume. Base on the review paper on the experimental findings provided by Referee 1, there will be great changes in $NO_2$ content and associated reaction in pathway, such as bigger stacking density will inhibit the thermal decomposition of RDX because they remove catalysts. We believe these experiment result in early years is also can be well explained by the importantly foundlings provided by W. A. Goddard et al via DFT methods（https://doi.org/10.1002/jcc.23893 and https://doi.org/10.1039/C4TA05676K）, where they found that the stability of the crystal will increase as the packing density increasing for DTTO, a high energetic material.*